Articles in PressS. Am J Physiol Renal Physiol (February 18, 2015). doi:10.1152/ajprenal.00591.2014
F-00591-2014-R

The Swan-Neck Lesion: Proximal Tubular Adaptation to Oxidative Stress in Nephropathic Cystinosis

Carolina I. Galarreta[1]

Michael S. Forbes[1]

Barbara A. Thornhill[1]

Corinne Antignac[2]

Marie-Claire Gubler[2]

Nathalie Nevo[2]

Michael P. Murphy[3]

Robert L. Chevalier[1]

[1]Department of Pediatrics, University of Virginia, Charlottesville, United States

[2]Inserm U1163, Laboratory of Hereditary Kidney Diseases, Paris, France

[3]MRC Mitochondrial Biology Unit, Cambridge, United Kingdom.

Running Head: Swan-neck lesion and oxidative stress in cystinosis

Address for correspondence:

Robert L. Chevalier, M.D.

Department of Pediatrics

University of Virginia, Box 800386

Charlottesville, VA 22908 U.S.A.

Tel: 434 924 5093

Fax: 434 982 3561

E-mail: RLC2M@virginia.edu

Abstract

Cystinosis is an inherited disorder resulting from a mutation in *CTNS*, causing progressive proximal tubular cell flattening, the "swan-neck lesion" (SNL) and eventual renal failure. To determine the role of oxidative stress in cystinosis, histologic sections of kidneys from C57BL/6 *Ctns*$^{-/-}$ and wild-type mice were examined by immunohistochemistry and morphometry from 1 week to 20 months of age (mo). Additional mice were treated from 1 to 6 mo with vehicle or mitoquinone (MitoQ), an antioxidant targeted to mitochondria. The leading edge of the SNL lost mitochondria and superoxide production, and became surrounded by thickened tubular basement membrane. Progression of the SNL as determined by *Lotus tetragonolobus* staining accelerated after 3 mo, but was delayed by treatment with MitoQ (38±4% vs. 28±1%, $p<0.01$). Through 9 mo, glomeruli retained renin staining and intact macula densa while SNL expressed transgelin, an actin-binding protein, but not kidney injury molecule-1 (KIM-1) or cell death (TUNEL). After 9 mo, clusters of proximal tubules localized oxidative stress (4-hydroxynonenal binding), expressed KIM-1, and underwent apoptosis (TUNEL), leading to formation of atubular glomeruli and accumulation of interstitial collagen (picrosirius). We conclude that nephron integrity is initially maintained in the *Ctns*$^{-/-}$ mouse by adaptive flattening of cells of the SNL, with reduced mitochondria, upregulation of transgelin, and thickened basement membrane. This adaptation ultimately fails in adulthood, with proximal tubular disruption, formation of atubular glomeruli, and renal failure. Antioxidant treatment targeted to mitochondria delays initiation of the SNL, and may provide therapeutic benefit in cystinotic children.

Key words: cystinosis, swan-neck lesion, oxidative injury, proximal tubule, Mitoquinone

51 **Introduction**

52

53 Cystinosis is an inherited metabolic disorder attributable to a mutation in *CTNS*, a
54 lysosomal transporter. The resulting intracellular cystine accumulation leads to multiple organ
55 dysfunction, including the development of Fanconi syndrome due to proximal tubular cystine
56 uptake. Therapy with cysteamine can delay, but not prevent, eventual renal failure in the second
57 or third decade of life (34). In cystinotic children, flattening of proximal tubular cells develops
58 between 6 and 12 months of age, creating a narrowed initial proximal tubule segment, the so-
59 called "swan-neck lesion" (SNL) (31). The proximal tubule is responsible for reclaiming the
60 majority of glomerular filtrate, which is accomplished by sodium transport fueled by ATP. The
61 initial segment of the proximal tubule reabsorbs most filtered amino acids, phosphate, and
62 glucose. The mechanisms responsible for proximal tubular dysfunction in cystinosis have not
63 been elucidated, but mitochondrial and oxidative injury are likely candidates (26, 47).

64 The study of the pathogenesis of cystinosis had been hampered by the lack of an animal
65 model manifesting the clinical renal phenotypic progression (7). This was solved by the
66 generation of *Ctns*$^{-/-}$ mice using a C57BL/6 genetic background: this strain develops Fanconi
67 syndrome by 2 months, SNL by 6 months, and decreasing glomerular filtration rate (GFR) by 10
68 months of age (35). More recent studies utilizing this *Ctns*$^{-/-}$ strain have revealed loss of
69 proximal tubular apical transporters and loss of tight junction integrity prior to the development
70 of SNL (19, 40).

71 Murine unilateral ureteral obstruction (UUO) has become the most widely-used model of
72 chronic kidney disease, with interstitial collagen deposition serving as an end-point for
73 measurement of experimental interventions (9). Recent morphometric studies of UUO have
74 demonstrated, however, that proximal tubular oxidative stress, mitochondrial loss and cell

death precede the interstitial changes (15, 17). Following 2 weeks of complete UUO, over 60% of proximal tubular mass is lost, concomitant with the formation of atubular glomeruli (15). A recent study of kidneys from cystinotic patients undergoing renal transplantation revealed widespread formation of atubular glomeruli—the end-stage of the SNL (30). These results, as well as a review of the glomerulotubular junction in many renal disorders (8), underscore the susceptibility of the proximal tubule in a broad spectrum of acute and chronic renal injury. The present study of the *Ctns*$^{-/-}$ mouse was designed to apply immunohistochemical and morphometric techniques to determine the sequence of epithelial cellular responses along the SNL and to measure the proximal tubular response to antioxidant therapy directed at the mitochondria.

MATERIALS AND METHODS

Experimental Animals. Studies were performed in *Ctns*-null mice (*Ctns* $^{-/-}$) generated on a C57BL/6 background and compared to C57BL/6 (wild-type) animals (35). Initial studies were performed on renal tissue from 15 *Ctns* $^{-/-}$ mice aged 3 to 20 months provided by C. Antignac and M.-C. Gubler. The remaining animals were bred at the University of Virginia Animal Care Facility from *Ctns* $^{-/-}$ stock obtained from C. Antignac and from C57BL/6 wild-type mice. Kidneys from 29 *Ctns*$^{-/-}$ and 39 age-matched wild-type animals were harvested at 1, 2, 3, and 4 weeks and 3, 6, 9, 12, and 15-16 months of age. Because the incidence of tall *Lotus* lectin-staining parietal cells lining the urinary pole of Bowman's capsule differs significantly between male and female mice older than 1 month (12), both sexes of mice were used for animals harvested before the first month of age, whereas only male mice were utilized for morphometric studies in older animals. Animal care and experimental procedures were conducted in accordance with approved protocols, including those by the University of Virginia Animal Care and Use Committee.

Tissue harvesting and processing. Animals were anesthetized with Avertin (2,2,2-tribromoethanol (Sigma-Aldrich) or pentobarbital sodium-phenytoin sodium solution (Euthasol: Virbac, Ft. Worth, TX). The majority of kidneys intended for paraffin embedment were perfused sequentially with nitroblue tetrazolium (NBT) in HBSS followed by formalin, as previously described (15). Formalin-fixed kidneys were embedded in paraffin and sectioned on a Leica RM2155 microtome at thicknesses ranging from 2-10 μm.

For plastic embedment, kidneys were transcardially perfused with PBS followed by 2.5% glutaraldehyde in PBS, or with NBT/HBSS followed by 2.5% glutaraldehyde in HBSS, pH 7.4. The majority of glutaraldehyde-fixed kidneys were sliced into 50-μm sections with a vibrating microtome (D.S.K Microslicer DTK-3000, Ted Pella, Inc., Redding CA), postfixed in osmium tetroxide, infiltrated with Poly/Bed 812 resin (Polysciences, Warrington PA) and embedded on microscope slides as previously described (14).

Glass knives mounted on a Sorvall MT-2B ultramicrotome were used to prepare semithin sections (0.1-0.2 μm), which were affixed to slides and stained with alkaline toludine blue or alcoholic basic fuchsin. The utilization of such semithin sections constitutes an optimal technique for examining relatively large areas with clear recognition of such small features as cystine crystals and autophagic vacuoles that would be obscured by superposition in conventional paraffin sections. All sections were examined and photographed with a Leica DMLS compound light microscope (Leica Microsystems, Wetzler, Germany) equipped with a QColor 3 digital camera (Olympus Corp., Valley, PA).

Staining. Antibodies and other reagents are listed with source and primary antibody dilution (where applicable) in the *Table.* Apoptotic cells were identified by TUNEL staining, basement membranes were stained with the periodic-acid Schiff (PAS) technique, and collagen with picrosirius red. *Lotus tetragonolobus* agglutinin staining was utilized to quantitate volume

124 fraction of mature proximal tubules ($V_{V(PT)}$) and the percentage of Lotus-staining glomerular
125 capsules (a measure of glomerulotubular integrity) (15, 17). Reactive oxygen species consistent
126 with mitochondrial superoxide formation was shown by the deposition of diformazan crystals
127 resulting from reduction of perfused nitroblue tetrazolium (10, 17). Oxidative stress was
128 localized by immunostaining for proteins complexed with 4-hydroxynonenal (4-HNE), a cytotoxic
129 product of lipid peroxidation (38). Tubular injury was identified by antibody to kidney injury
130 molecule-1 (KIM-1, upregulated in proximal tubule in response to a toxic stimulus) (4).

131 Alterations within epithelial cells of Bowman's capsule and the contiguous proximal
132 tubule were studied with immunostaining for megalin, α-smooth-muscle actin (α-SMA), vimentin,
133 nestin, or transgelin. The presence of the juxtaglomerular apparatus of nephrons was
134 demonstrated by staining for renin.

135 **Morphometry.** Morphometric determinations of volume fractions of proximal tubules and
136 collagen contribution were made, respectively, in *Lotus* and picrosirius-red stained median
137 sagittal sections, using microscopic fields at X400 magnification as previously detailed (16).
138 For glomerular areas (both capsule and tuft), 40 glomeruli per kidney section were measured in
139 a manner designed to sample the entire cortical thickness (48). These measurements were
140 made by means of ImagePro Plus 5.1 or 7.0 image-analysis software (Media Cybernetics, Silver
141 Spring, MD). Area of Bowman's space was determined by subtracting the glomerular tuft area
142 from total area within Bowman's capsule. Measurement of the fraction of *Lotus*-stained
143 glomeruli was performed as described previously (15). Using serial sectioning, atubular
144 glomeruli were demonstrated in older *Ctns*$^{-/-}$ mice by the lack of continuity between Bowman's
145 capsule and proximal tubule (20).

146 **Mitoquinone (MitoQ) studies.** *Ctns*$^{-/-}$ mice were treated with MitoQ (MS-010; 20-25% w/w
147 mitoquinone complex with beta-cyclodextrin, provided by M.P. Murphy) or vehicle dTPP (decyl-

triphenylphosphonium, Santa Cruz Biotechnology, sc-264801) beginning at either 1 month or 3 months of age (n = 8-9 each group); kidneys from all mice were harvested at 6 months of age. Mice were housed 2-3 per cage, and were weighed weekly. They received either dTPP at a concentration of 125 μM or MitoQ in drinking water, *ad libitum.* Administration to mice of 500 μM MitoQ in drinking water results in tissue concentrations of MitoQ of 20±2 pmol/g wet weight of liver, and produces no evident toxicity when administered at this dose for up to 28 weeks (41). Salutary effects have been reported following cardiac ischemia/reperfusion in rats, and for diabetic nephropathy in $Ins2^{+/-AkitaJ}$ mice (1, 6). The concentration of MitoQ was initially 100 μM and was gradually increased over 7-10 days to a final concentration of 500 μM which was continued for the duration of the study. MitoQ and dTPP stock solutions were prepared using sterile filtered tap water, stored at 4°C, and protected from light. Water intake was measured daily. An additional group of 8 mice received sterile filtered water and were harvested at 6 months. Kidneys were harvested and processed for staining with *Lotus tetragonolobus* as described above. Urine samples (50-100 μl) from wild-type mice and from mice treated with dTPP or MitoQ were collected from individual animals prior to sacrifice, and stored at -20°C until measurement of urine retinol-binding protein and creatinine by immunoassay (DetectX, Arbor Assays, Ann Arbor, MI). Kidney tissue concentration of MitoQ was determined in 6 mice receiving MitoQ at a concentration of 500 μM for 3 weeks (41).

Statistical analysis. The SigmaStat program v. 3.0 (Aspire Software International, Ashburn, VA) was utilized. Age-matched groups were compared using t-test for normally distributed data, or Mann-Whitney rank-sum test for data not normally distributed. Two-way ANOVA was used to compare the effects of MitoQ and duration of treatment on initiation of the SNL. Statistical significance was defined as $P < 0.05$.

RESULTS

Initiation of the swan-neck lesion (SNL). In mature wild-type ("control") C57BL/6 mice, the glomerulotubular junction was characterized by tall, mitochondrion-rich epithelial cells extending from the proximal tubule onto the urinary pole of Bowman's capsule, making an abrupt transition to flat parietal epithelial cells (Fig. 1A). In the cystinotic mouse the tall epithelial cells were modified to become extremely flattened (Fig. 1B), forming the definitive swan-neck lesion (SNL).

Reactive oxygen species consistent with superoxide produced by mitochondrial metabolism were localized by the presence of blue diformazan crystals following perfusion with nitroblue tetrazolium (10). Diformazan was distributed along the basal surfaces of the tall epithelium of wild-type glomerulotubular junctions and proximal tubules (Fig. 1C), but was absent from the cells forming the SNL in cystinotic nephrons (Fig. 1D). In wild-type kidneys, *Lotus tetragonolobus* lectin was typically bound within the apical cytoplasm of the tall parietal epithelial cells of Bowman's capsule, but did not stain the thin parietal cells (Fig. 1E). In contrast, the epithelium lost its affinity for *Lotus* staining along the flattening SNL (Fig. 1F). The distribution of megalin (LRP2), a membrane-associated binding receptor, was similar to that of *Lotus* lectin in control kidneys (Fig. 1G), but unlike *Lotus*, megalin positivity was retained in the flattened cells of the SNL in cystinotic nephrons (Fig. 1H).

The basement membrane of wild-type nephrons consisted of a thin coating along the basal surfaces of the glomerular capsule, the glomerulotubular junction, and the contiguous proximal tubule (Fig. 1I); in cystinotic nephrons, the basement membranes of both the glomerulotubular junction and proximal tubule were considerably thickened, their augmentation corresponding to the original positions of the tall cells (Fig. 1J).

Progression of the swan-neck lesion (3-9 months). By 3 months of age, *Lotus* staining of proximal tubules of C*tns*$^{-/-}$ mice revealed considerable internephron heterogeneity (Fig. 2A-D).

In both wild-type and *Ctns*$^{-/-}$ mice younger than one month of age, more than 50% of glomeruli lacked *Lotus* positivity, reflecting immaturity of the glomerulotubular junction at this age (Figs. 2E and 2F). With postnatal maturation, the fraction of *Lotus*-positive glomerular capsules increased, such that through the first month of life it rose from 40 to 80% in wild-type mice, and from 30 to 60% in cystinotics (Figs. 2E, 2G and 2I). After three months, however, there was a progressive decrease in the fraction of *Lotus*-positive glomerular capsules with increasing age in cystinotic mice, but not in wild-type mice (Fig. 2E, 2H and 2J). The wide variation in fraction of *Lotus*-positive glomerular capsules among Ctns $^{-/-}$ kidneys indicates that the timing of initiation of the SNL among different nephrons is highly variable (Figs. 2I and 2J).

Antioxidant treatment delays initiation of the swan-neck lesion (2-6 months). To determine the role of proximal tubular mitochondrial oxidative stress in the initiation of the SNL, *Ctns*$^{-/-}$ mice were provided with mitoquinone (MitoQ) or vehicle (dTPP) in drinking water from 3 to 6 months (short-term) or 1-6 months of age (long-term) (Fig. 3A). In 6 mice receiving MitoQ at 500 μM in drinking water for 3 weeks, kidney tissue concentration was 27.3±3.2 pmol/g. As shown in Figure 3B, compared to those receiving vehicle (28.6±2.1%), *Ctns*$^{-/-}$ mice receiving MitoQ maintained a greater fraction of intact glomerulotubular junctions (37.4±2.1%) ($p<0.01$, 2-way ANOVA), consistent with a salutary effect of mitochondrial antioxidant therapy. There was no difference in fraction of intact glomerulotubular junctions between short-term (33.2±2.1%) and long-term treatment (32.8±2.1%) ($p=0.9$, 2-way ANOVA). Daily water consumption was 17% greater in mice receiving MitoQ (2.7 ± 0.1 ml/day) than dTPP (2.3 ± 0.1 ml/day) ($p<0.05$); body weight was 13% higher in mice receiving MitoQ (27.7±0.4 g) than dTPP (24.4±0.5 g) ($p<0.05$), but left kidney weight did not differ between MitoQ (203±5 mg) and dTPP (198±7 mg) groups. Body weight and fraction of intact glomerulotubular junctions were greater in mice receiving water without vehicle than water containing dTPP ($p<0.05$), but kidney weight was not different. There was no difference in urinary retinol-binding protein/creatinine concentration ratio between

221 dTPP (13.7 ± 1.7, N = 13) and MitoQ (9.9 ± 1.4 ng/ml, N = 19) Ctns $^{-/-}$ groups; or untreated wild-
222 type mice (10.0 ± 2.5, N = 6).

223 **Preservation and remodeling of glomerulotubular structures following formation of the**
224 **swan-neck lesion (3-9 months).** Despite marked flattening of parietal epithelial cells lining the
225 urinary pole of Bowman's capsule, much of the glomerular morphology remained unchanged,
226 with conservation of juxtaglomerular renin production (Figs. 4A, 4B) and an intact macula densa
227 (Fig. 4C).

228 Transgelin, a cytoskeletal protein associated with stabilization of cellular structure, while
229 abundant in vascular smooth muscle cells, was rarely expressed in the glomerular capsules or
230 proximal tubular epithelium of wild-type mice (Fig. 5A). In contrast, transgelin positivity appeared
231 in nephrons of cystinotic kidneys at 6 months of age, and by 9 months was present in many of
232 the glomerular capsules of cystinotic kidneys (Fig. 5B, 5C) as well as in the flat swan-neck
233 epithelium itself (Fig. 5C). The association of transgelin with α-smooth muscle actin (α-SMA),
234 as seen in serial sections (Figs. 5D, 5E), is consistent in arteriolar vessels, with some
235 colocalization seen in glomerular capsules (Figs. 5F, 5G) and occasionally in swan-neck
236 epithelium (not shown). Vimentin and nestin immunostaining were also found in the SNL (not
237 shown).

238 Regardless of genotype, the *Lotus*-positive proximal tubular fraction of cortical
239 parenchyma increased with maturation throughout the first 3 months (Figs. 6A and 6E) but
240 declined thereafter in *Ctns*$^{-/-}$ mice (Figs. 6B-6E). By 20 months, many Lotus-stained proximal
241 tubules of *Ctns*$^{-/-}$ mice had become dilated (Fig. 6D). There was no significant effect of MitoQ on
242 proximal tubular volume fraction at 6 months (Fig. 3C), consistent with only a small reduction in
243 this parameter at this age in *Ctns*$^{-/-}$ vs. wild-type mice (Fig.6E).

Late events: Bowman's capsule dilatation, tubule damage, generation of atubular glomeruli, interstitial collagen accumulation, and cast material formation. As early as 9 months of age, degenerative zones began to appear in cystinotic kidneys (example shown in Fig. 7). Within these zones, shrunken proximal tubules exhibited apoptosis (Fig. 7A), blue diformazan incorporation (Fig. 7B), upregulation of KIM-1 (Fig. 7C) and oxidative stress (4-HNE, Fig. 7D). In addition to these changes, after 12 months of age, *Ctns*$^{-/-}$ mice accumulated PAS-positive cast material in papillary collecting ducts (Figs 7E and 7F). The extent of the lesions increased with age, and included interstitial cellular infiltrate, dilatation of tubules and Bowman's space, and crowding of glomeruli (Fig. 8A, 8B), whose capsules often expressed α-smooth muscle actin (cf. Fig. 5G). This was associated with the formation of atubular glomeruli, demonstrated conclusively by serial sectioning (Fig.8C). In older kidneys of *Ctns*$^{-/-}$ mice, basement membranes were thickened both around the glomerulus and surrounding atrophic proximal tubules (Fig. 9A). A marked increase in Sirius-positive collagen staining was evident after 9 months of age (Fig. 9B, C).

Discussion

Since the initial report of the "swan-neck lesion" (SNL) in a child with nephropathic cystinosis (11), the biochemistry of the disorder has been elucidated, and the responsible gene has been identified (47). Despite these advances, the relationship of lysosomal cystine accumulation to proximal tubular dysfunction and progression of the nephropathy has not been defined. Although our understanding of the pathogenesis of this disorder has been significantly expanded by the recent development of a mouse model of nephropathic cystinosis, the SNL continues to be regarded as a form of tubular atrophy (19). The present study in *Ctns*$^{-/-}$ mice

268 indicates that rather than being the result of a purely degenerative process, the SNL is a
269 consequence of multiple cellular adaptations by the proximal tubule.

270 **The role of mitochondrial oxidative stress in the initiation of the SNL.** Data regarding ATP
271 metabolism and cell oxidation in cystinosis have been generated largely from *in vitro* studies
272 (47). However, whereas ATP metabolism *in vitro* is largely dependent on glycolytic activity, ATP
273 *in vivo* is generated by mitochondrial oxidative phosphorylation, associated with generation of
274 reactive oxygen species (47). For these reasons, we sought to localize mitochondrial function
275 along the nephrons of cystinotic mice during evolution of the SNL. As shown in the present
276 study, maturation of the glomerulotubular junction generally proceeds in cystinotic mice from
277 birth through 3 months of age, albeit at a diminished rate (Fig. 2E).

278 The use of antioxidants in chronic diseases such as heart failure, diabetes, and chronic
279 kidney disease have thus far been disappointing, results likely attributable to the lack of efficient
280 targeting of compounds to mitochondria (43). Mitoquinone (MitoQ), a small-molecule antioxidant
281 compound, is specifically sequestered within mitochondria: its conjugation to
282 triphenylphosphonium (TPP), a lipophilic cation, results in concentrations 100-500-fold higher in
283 the mitochondria than in the plasma (44). Notably, oral MitoQ decreased liver damage in a
284 phase II study of hepatitis C patients, showing promise for its clinical use (21). The results of the
285 present study reveal a significant reduction of the initiation of the SNL in mice receiving MitoQ
286 compared to those receiving dTPP vehicle, consistent with a role for mitochondrial oxidative
287 stress in this process. The interval between 3 and 6 months of age (common to both short-term
288 and long-term MitoQ treatment groups) is the period of initiation of the swan-neck lesion (Fig
289 2E). The lack of additional benefit from the earlier initiation of MitoQ treatment in the long-term
290 group suggests that susceptibility of the proximal tubule to stimuli that initiate the phenotypic
291 changes in epithelial cells does not develop until 3 months of age. The inter-animal variation in
292 the rate of SNL initiation for 6 month-old *Ctns*$^{-/-}$ mice (Fig. 2E) would preclude estimation of the

rate of SNL extension in individual nephrons, however. Maintenance of *Lotus*-positive proximal tubule volume fraction by *Ctns*$^{-/-}$ mice (Fig. 6E) likely reflects compensatory proximal tubular growth distal to the SNL (19). Such compensation would account for the lack of effect of *CTNS* gene activity or of MitoQ on urinary concentration of retinol-binding protein, an index of megalin-mediated proximal tubular protein reabsorption.

Nephron integrity is maintained in the early phase of cystinosis: the role of the SNL. The SNL could be formed by either phenotypic transition of tall proximal tubular cells *in situ*, or by migration of flat parietal epithelial cells from the vascular pole of Bowman's capsule down the tubule (19). In the present study, the tubular basement membrane underlying flattened glomerulotubular junctions in *Ctns*$^{-/-}$ mice becomes particularly thickened (unlike that of parietal epithelial cells lining the vascular pole of Bowman's capsule in either strain) (Fig. 1B, 1J). Although *Lotus* lectin staining is lost along the flattening cells of the glomerulotubular junction of *Ctns*$^{-/-}$ mice, megalin staining persists (Figs 1G, 1H). These changes are thus consistent with a phenotypic transition of proximal tubular cells along the leading edge of the SNL rather than migration of parietal epithelial cells from Bowman's capsule down the proximal tubule. Despite its persistence, megalin in flattened cells is unlikely to contribute significantly to uptake of cystine from tubular fluid along the SNL, which lacks an intact tubulovesicular system or a significant source of energy (mitochondria). Moreover, megalin-expressing proximal tubular cells are more susceptible to injury resulting from experimental renal disease than are megalin-deficient proximal tubular cells (32).

In the normal nephron, high transmural hydraulic pressure in Bowman's capsule and the proximal tubule generates considerable tension, which is countered by a basement membrane which is thicker than that in more distal segments (42). Additional basement membrane is produced by tubular cells undergoing phenotypic transition, a process that should enhance tensile strength of the SNL (45). In combination with its enhanced tensile strength, the

considerably reduced overall diameter of the SNL segment would reduce wall tension compared to Bowman's capsule (law of LaPlace: tension = pressure x radius). The SNL therefore becomes a conduit for tubular fluid to downstream segments which must initially compensate for the loss in reabsorptive function. The development of the Fanconi syndrome reveals that such compensation is incomplete, and ultimately fails when the S3 segment becomes overwhelmed.

Despite the profound morphological alterations taking place along the proximal tubule of *Ctns*$^{-/-}$ mice, the glomerular tuft remains normal in appearance throughout life (Fig. 4). Maintenance of a renin-producing juxtaglomerular apparatus and an apparently normal macula densa points to an intact tubuloglomerular feedback mechanism. Transgelin, an actin-binding protein of the calponin family and an early marker of smooth muscle differentiation, contributes to stabilization of cell structure by interaction with actin (2, 22). Its upregulation by flattened cells of the SNL is also consistent with an adaptive response to metabolic and oxidative stress in the cystinotic kidney.

The response of the proximal tubule in cystinosis differs markedly from that resulting from unilateral ureteral obstruction (UUO), the most widely-used animal model of chronic kidney disease (9). During the course of 2 weeks of complete UUO in the adult mouse, proximal tubules accumulate 4-HNE, upregulate KIM-1(Forbes, unpublished observations), and undergo massive cell loss by necrosis, apoptosis, and autophagy, along with formation of atubular glomeruli (15, 17). These cellular responses can be characterized using a paradigm originally developed by Cannon, and adapted by Goligorsky, namely *fight or flight* (23). In this context, as opposed to the tubular *atrophy* which results from UUO ("flight"), the SNL instead represents an *adaptation* to cystine accumulation ("fight"), which postpones progression to renal failure. Kritz et al. have proposed an analogous hypothesis to account for podocyte foot process effacement in glomerular disorders: rather than being a manifestation of injury, the phenotypic transition of

342 podocytes reduces their detachment from the glomerular basement membrane, thereby slowing
343 nephron loss (29).

344 **Early nephron adaptations fail in the late phase of cystinosis: tubular atrophy and**
345 **formation of atubular glomeruli.** The proximal tubule is well-known to be more vulnerable to
346 hypoxic and oxidative stress than are downstream nephron segments, being more dependent
347 on mitochondrial oxidative phosphorylation, but containing fewer endogenous antioxidants (3,
348 26, 28). As is evident from morphometric analysis, the SNL adaptations employed during the
349 first 6 months are not sufficient to prevent the eventual proximal tubular loss that is notable by
350 12 months (Fig. 7). Atrophic proximal tubules that stain intensely for TUNEL, 4-HNE and KIM-1
351 reflect ongoing oxidative stress and activation of apoptotic pathways, leading ultimately to the
352 formation of atubular glomeruli. By 12 months, the predominant response of the cystinotic
353 proximal tubule has made a transition from “fight” to “flight”. It has been noted that multiple
354 death pathways have developed as a result of evolution, presumably because a single
355 mechanism would be subject to hijacking by opportunistic parasitic organisms (36). Moreover,
356 metabolism and cell death are intertwined: many proteins that mediate metabolic functions act
357 as transducers of cell death-regulatory signals at “metabolic checkpoints” (24). When metabolic
358 stress becomes severe and protracted in the S3 segment as the SNL extends distally, metabolic
359 checkpoints in this segment switch to initiate cell death (24). This is reflected also by
360 progressive activation of inflammasomes in kidneys of *Ctns*$^{-/-}$ mice between 5 and 17 months of
361 age, which presumably contribute to interstitial fibrosis present in terminal phases of the
362 nephropathy (39). Widespread formation of atubular glomeruli was reported in six 10-24 year-
363 old patients with end-stage renal disease resulting from cystinosis (30). As in the present murine
364 study, formation of atubular glomeruli is presumed to represent the final stage of the SNL
365 development.

366 **The *Ctns*$^{-/-}$ mouse as a model of human nephropathic cystinosis.** Cystinosis is a rare
367 disorder, with a prevalence of approximately 1:100,000 across the world (34). Because of the
368 paucity of available data, constructing the progression of renal lesions in clinical cystinosis has
369 necessarily been based on a few studies of small numbers of patients. A report of two cystinotic
370 children undergoing renal biopsy at 5-6 months and again at 12-14 months of age revealed that,
371 although Fanconi syndrome was present at 5-6 months, the SNL appeared only in the second
372 biopsies (31). In five cystinotic patients 1-5 years of age, creatinine clearance was reduced by
373 approximately 50% (27), while kidney biopsies from six cystinotic children 2-12 years of age
374 revealed SNL in 36-89% of nephrons, with significant variation observed among individual
375 patients and nephrons (13). Kidneys from six cystinotic patients 10-24 years of age undergoing
376 renal transplantation revealed that 69% of glomeruli were atubular, 30% had SNL and only 1%
377 were normal (30). These data were used to generate a chronology for progression of cystinosis
378 in children (Fig. 10). The original description of the C57BL/6 *Ctns*$^{-/-}$ mouse noted the
379 development of Fanconi syndrome by 2 months of age, no change in creatinine clearance by 9
380 months of age, but a decrease by 50% at 10-18 months (35). A chronology for the mouse model
381 can be fitted to the sequence of events depicted for human cystinosis, with 12 months in the
382 mouse being equivalent to 3 years of age in the child (Fig. 10). Although there are many
383 apparent similarities in the evolution of renal adaptations and progression of injury in human and
384 murine *CTNS* mutations, the onset of advanced renal insufficiency begins in childhood in the
385 former, but only in adulthood in the mouse. Glomerular structural and functional changes
386 (including multinucleated podocytes and heavy proteinuria) develop in human cystinosis, but not
387 in the C57BL/6 *Ctns*$^{-/-}$ mouse (46). Most importantly, the expression of a renal phenotype in the
388 mutant mouse is largely dependent on its genetic background, underscoring the importance of
389 modifier genes (35).

A recent report highlights proximal tubular dysfunction resulting from dedifferentiation preceding initiation of the SNL, with S3 segment compensatory uptake of labeled proteins by the *Ctns*$^{-/-}$ mouse (19). Additional adaptive mechanisms include lysosomal clearance of cystine into urine and ongoing proximal tubular repair (19). Although Raggi et al. report SNL in <5% of nephrons in 6 month-old *Ctns*$^{-/-}$ mice, quantitative morphometry was not employed (40). With the use of a morphometric method that employs staining with *Lotus* lectin, the present study shows initiation of the SNL in approximately 50% of nephrons between 3 and 6 months (Fig. 2). The results of the present study suggest that the term swan-neck “lesion” is actually a misnomer, as it does not have all the characteristics of definitive tubular atrophy: cells retain megalin, remain adherent to basement membrane, and do not express KIM-1. By taking on a reduced diameter, expressing transgelin, developing a thickened basement membrane, and reducing mitochondrial volume, the formation of the SNL can be viewed as an *adaptation* to injurious stimuli (Fig. 10). Cells of the SNL adapt to oxidative stress by flattening with loss of apical cystine binding and mitochondrial loss, temporarily preventing ongoing cystine uptake and further oxidative injury in that segment. However, this temporizing measure, as well as the adaptive responses by downstream proximal tubular segments reported by Gaide Chevronnay et al. (19), ultimately fail to preserve homeostasis.

Proximal tubular phenotypic changes of the cystinotic SNL may be analogous to those resulting from combined renal artery stenosis and angiotensin converting enzyme inhibition in the rat (25). Proximal tubular diameter in this model of renovascular hypertension is also reduced with flattened epithelial cells characterized by reduced brush border, decreased ATPase and lysosome activity, and loss of mitochondria (25). However, these changes are reversible following release of the vascular clip and withdrawal of enalapril, making this a model of “renal hibernation” (25). As noted above, cellular responses to stress are determined by metabolic checkpoints (24), and the evolution of regulatory mechanisms has been shaped by

natural selection through the balancing of costs and benefits of responding versus not responding to ambiguous cues (33). Although formation of the SNL has been regarded as a "maladaptive" response to cystine accumulation, the process of evolution involves a balance between physiological adaptations and buffering by enhanced robustness that protects against perturbations and increases reproductive fitness (18). The short-term benefits (but eventual failure) of preserving integrity of the proximal tubule by formation of the SNL are analogous to those accrued by glomerular hyperfiltration following reduction in renal mass (5), or podocyte foot process effacement in glomerular disorders (29). Although these nephron responses have been viewed as hallmarks of disease (and therefore maladaptive), the evolutionary perspective confers additional value by revealing the operation of cellular regulatory responses.

We conclude that additional studies of the *Ctns*$^{-/-}$ mouse should be directed to the first 3-6 months of life, prior to the development of irreversible tubular injury (Fig. 10). Despite the initiation of SNL during this period, the maintenance of tubular fluid flow and of epithelial cells that remain adherent to an intact basement membrane should permit remodeling of a fully functioning S1 segment by therapies designed to reduce cystine overload and oxidative mitochondrial injury. Cysteamine has already proven effective in attenuating the progression of renal lesions in cystinosis, presumably due to its antioxidant properties as well as reduction of intracellular cystine stores (37). As demonstrated by the present study, treatment with antioxidants targeted to mitochondria may provide additional therapeutic benefit.

References

1. **Adlam VJ, Harrison JC, Porteous CM, James AM, Smith RAJ, Murphy MP and Sammut IA**. Targeting an antioxidant to mitochondria decreases cardiac ischemia-reperfusion injury. *FASEB J* 19: 1088-1095, 2005.

2. **Assinder SJ, Stanton JAL and Prasad PD**. Transgelin: An actin-binding protein and tumour suppressor. *Int J Biochem Cell Biol* 41: 482-486, 2008.

3. **Bagnasco S, Good D, Balaban R and Burg M**. Lactate production in isolated segments of the rat nephron. *Am J Physiol Renal Physiol* 248: F522-F526, 1985.

4. **Bonventre JV**. Kidney injury molecule-1: a urinary biomarker and much more. *Nephrol Dial Transplant* 24: 3265-3268, 2010.

5. **Brenner BM**. Chronic renal failure: A disorder of adaptation. *Perspect Biol Med* 32: 434-444, 1989.

6. **Chacko BK, Reily C, Srivastava A, Johnson MS, Ye Y, Ulasova E, Agarwal A, Zinn KR, Murphy MP, Kalyanaraman B and Darley-Usmar V**. Prevention of diabetic nephropathy in Ins2(+/)-(AkitaJ) mice by the mitochondria-targeted therapy MitoQ. *Biochem J* 432: 9-19, 2010.

7. **Cherqui S, Sevin C, Hamard G, Kalatzis V, Sich M, Pequignot MO, Gogat K, Abitbol M, Broyer M, Gubler MC and Antignac C**. Intralysosomal cystine accumulation in mice lacking cystinosin, the protein defective in cystinosis. *Mol Cell Biol* 22: 7622-7632, 2002.

8. **Chevalier RL and Forbes MS**. Generation and evolution of atubular glomeruli in the progression of renal disorders. *J Am Soc Nephrol* 19: 197-206, 2008.

9. **Chevalier RL, Forbes MS and Thornhill BA**. Ureteral obstruction as a model of renal interstitial fibrosis and obstructive nephropathy. *Kidney Int* 75: 1145-1152, 2009.

10. **Chien CT, Lee P-H, Chen C-F, Ma M-C, Lai M-K and Hsu S-M**. De novo demonstration and co-localization of free-radical production and apoptosis formation in rat kidney subjected to ischemia/reperfusion. *J Am Soc Nephrol* 12: 973-982, 2001.

11. **Clay RD, Darmady EM and Hawkins M**. The nature of the renal lesion in the Fanconi syndrome. *J Path Bact* 65: 551-558, 1953.

12. **Crabtree C**. The structure of Bowman's capsule as an index of age and sex variations in normal mice. *Anat Rec* 79: 395-413, 1941.

13. **Fetterman GH, Fabrizio NS and Studnicki FM**. The study by microdissection of structural tubular defects in certain examples of the hereditary nephropathies. *Proc 3rd Int Congr Nephrol , Washington 1966* 2: 235-250, 1967.

14. **Forbes MS, Ghribi O, Herman MM and Savory J**. Aluminum-induced dendritic pathology revisited: Cytochemical and electron microscopic studies of rabbit cortical pyramidal neurons. *Ann Clin Lab Sci* 32: 75-86, 2002.

15. **Forbes MS, Thornhill BA and Chevalier RL**. Proximal tubular injury and rapid formation of atubular glomeruli in mice with unilateral ureteral obstruction: A new look at an old model. *Am J Physiol Renal Physiol* 301: F110-F117, 2011.

16. **Forbes MS, Thornhill BA, Galarreta CI, Minor JJ, Gordon KA and Chevalier RL**. Chronic unilateral ureteral obstruction in the neonatal mouse delays maturation of both kidneys and leads to late formation of atubular glomeruli. *Am J Physiol Renal Physiol* 305: F1736-F1746, 2013.

17. **Forbes MS, Thornhill BA, Minor JJ, Gordon KA, Galarreta CI and Chevalier RL**. Fight-or-flight: murine unilateral ureteral obstruction causes extensive proximal tubular degeneration, collecting duct dilatation, and minimal fibrosis. *Am J Physiol Renal Physiol* 303: F120-F129, 2012.

18. **Frank SA**. Maladaptation and the paradox of rubustness in evolution. *PLoS ONE* 2(10): e1021, 2007.

19. **Gaide Chevronnay HP, Janssens V, Van Der Smissen P, N'kuli F, Nevo N, Guiot Y, Levtchenko E, Marbaix E, Pierreux CE, Cherqui S, Antignac C and Courtoy PJ**. Time course of pathogenic and adaptation mechanisms in cystinotic mouse kidneys. *J Am Soc Nephrol* 25: 1256-1269, 2014.

20. **Galarreta CI, Grantham JJ, Forbes MS, Maser RL, Wallace DP and Chevalier RL**. Tubular obstruction leads to progressive proximal tubular injury and atubular glomeruli in polycystic kidney disease. *Am J Pathol* 184: 1957-1966, 2014.

21. **Gane EJ, Weilert F, Orr DW, Keogh GF, Gibson M, Lockhart MM, Frampton CM, Taylor KM, Smith RAJ and Murphy MP**. The mitochondria-targeted anti-oxidant mitoquinone decreases liver damage in a phase II study of hepatitis C patients. *Liver Int* 30: 1019-1026, 2010.

22. **Gerolymos M, Karagianni F, Papasotiriou M, Kalliakmani P, Sotsiou F, Charonis A and Goumenos DS**. Expression of transgelin in human glomerulonephritis of various etiology. *Nephron Clin Pract* 119: c74-c82, 2011.

23. **Goligorsky MS**. The concept of cellular "fight-or-flight" reaction to stress. *Am J Physiol Renal Physiol* 280: F551-F561, 2001.

24. **Green DR, Galluzzi L and Kroemer G**. Metabolic control of cell death. *Science* 345: DOI:10.1126/science.1250256, 2014.

25. **Grone H-J, Warnecke E and Olbricht CJ**. Characteristics of renal tubular atrophy in experimental renovascular hypertension: A model of kidney hibernation. *Nephron* 72: 243-252, 1996.

26. **Hall AM, Unwin RJ, Parker N and Duchen MR**. Multiphoton imaging reveals differences in mitochondrial function between nephron segments. *J Am Soc Nephrol* 20: 1293-1302, 2009.

27. **Jackson JD, Smith FG, Litman NN, Yuile CL and Latta H**. The Fanconi syndrome with cystinosis. Electron microscopy of renal biopsy specimens from five patients. *Am J Med* 33: 893-910, 1962.

28. **Kiyama S, Yoshioka T, Burr IM, Kon V, Fogo A and Ichikawa I**. Strategic locus for the activation of the superoxide dismutase gene in the nephron. *Kidney Int* 47: 536-546, 1995.

29. **Kriz W, Shirato I, Nagata M, LeHir M and Lemley KV**. The podocyte's response to stress: the enigma of foot process effacement. *Am J Physiol Renal Physiol* 304: F333-F347, 2013.

30. **Larsen CP, Walker PD and Thoene JG**. The incidence of atubular glomerluli in nephropathic cystinosis renal biopsies. *Mol Genet Metab* 101: 417-420, 2010.

31. **Mahoney CP and Striker GE**. Early development of the renal lesions in infantile cystinosis. *Pediatr Nephrol* 15: 50-56, 2000.

32. **Motoyoshi Y, Matsusaka T, Saito A, Pastan I, Willnow TE, Mizutani S and Ichikawa I**. Megalin contributes to the early injury of proximal tubule cells during nonselective proteinuria. *Kidney Int* 74: 1262-1269, 2008.

33. **Nesse RM**. Maladaptation and natural selection. *Quarterly Review of Biology* 80: 62-70, 2005.

34. **Nesterova G and Gahl WA**. Cystinosis: the evolution of a treatable disease. *Pediatr Nephrol* 28: 51-59, 2013.

35. **Nevo N, Chol M, Bailleux A, Kalatzis V, Morisset L, Devuyst O, Gubler MC and Antignac C**. Renal phenotype of the cystinosis mouse model is dependent upon genetic background. *Nephrol Dial Transplant* 25: 1059-1066, 2010.

36. **Nicotera P, Petersen OH, Melino G and Verkhratsky A**. Janus a god with two faces: death and survival utilise same mechanisms conserved by evolution. *Cell Death Differ* 14: 1235-1236, 2007.

37. **Okamura DM, Bahrami NM, Ren S, Pasichnyk K, Williams JM, Gangoiti JA, Lopez-Guisa JM, Yamaguchi I, Barshop BA, Duffield JS and Eddy AA**. Cysteamine modulates oxidative stress and blocks myofibroblast activity in CKD. *J Am Soc Nephrol* 25: 43-54, 2014.

38. **Picklo MJ, Amarnath V, McIntyre JO, Graham DG and Montine TJ**. 4-hydroxy-2(E)-nonenal inhibits CNS mitochondrial respiration at multiple sites. *J Neurochem* 72: 1617-1624, 1999.

39. **Prencipe G, Caiello I, Cherqui S, Whisenant T, Petrini S, Emma F and De Benedetti F**. Inflammasome activation by cystine crystals: Implications for the pathogenesis of cystinosis. *J Am Soc Nephrol* 25: 1163-1169, 2014.

40. **Raggi C, Luciani A, Nevo N, Antignac C, Terryn S and Devuyst O**. Dedifferentiation and aberrations of the endolysosomal compartment characterize the early stage of nephropathic cystinosis. *Hum Mol Genet* 23: 2266-2278, 2014.

41. **Rodriguez-Cuenca S, Cocheme HM, Logan A, Abakumova I, Prime TA, Rose C, Vidal-Puig A, Smith AC, Rubinsztein DC, Fearnley IM, Jones BA, Pope S, Heales SJR, Lam BYH, Neogi SG, McFarlane I, James AM, Smith RAJ and Murphy MP**. Consequences of long-term oral administration of the mitochondria-targeted antioxidant MitoQ to wild-type mice. *Free Rad Biol Med* 48: 161-172, 2010.

42. **Sakai T and Hijikata T**. Structural specializations of the basement membrane and their mechanical relevance to the kidney. *Contrib Nephrol* 95: 34-47, 1991.

43. **Sheu SS, Nauduri D and Anders MW**. Targeting antioxidants to mitochondria: A new therapeutic direction. *Biochim Biophys Acta* 1762: 256-265, 2006.

44. **Smith RAJ, Porteous CM, Gane AM and Murphy MP**. Delivery of bioactive molecules to mitochondria *in vivo*. *Proc Natl Acad Sci USA* 100: 5407-5412, 2003.

45. **Welling LW and Grantham JJ**. Physical properties of isolated perfused renal tubules and tubular basement membranes. *J Clin Invest* 51: 1063-1075, 1972.

46. **Wilmer MJ, Christensen EI, van den Heuvel LP, Monnens LA and Levtchenko EN**. Urinary protein excretion pattern and renal expression of megalin and cubulin in nephropathic cystinosis. *Am J Kidney Dis* 51: 893-903, 2008.

47. **Wilmer MJ, Emma F and Levtchenko EN**. The pathogenesis of cystinosis: mechanisms beyond cystine accumulation. *Am J Physiol* 299: F905-F916, 2010.

48. **Yoo KH, Thornhill BA, Forbes MS and Chevalier RL**. Compensatory renal growth due to neonatal ureteral obstruction: Implications for clinical studies. *Pediatr Nephrol* 21: 368-375, 2006.

572 **Acknowledgments**

573

574 This project was funded by a grant from the Cystinosis Research Foundation. M. P. Murphy has
575 an association with Antipodean Pharmaceuticals, a company that is commercializing
576 MitoQ. Jennifer Charlton performed assays of urine retinol binding protein, and Angela
577 Logan performed mass spectrometry assays of kidney tissue Mitoquinone. The technical
578 assistance of Hiwat Abate, Thy Nguyen, Akif Shameem, and YuChia Wang is gratefully
579 acknowledged. Portions of this study were presented in preliminary form at the annual
580 meeting of the Pediatric Academic Societies, Boston, MA, 2013; 4th International
581 Cystinosis Research Symposium, Irvine, CA, 2014; and the annual meeting of the
582 American Society of Nephrology, Philadelphia, PA, 2014.

583

584

585 **Table. Antibodies used in immunohistochemical studies**

Antibody	Source	Product No.	Host/MC/PC	Dilution
Apoptag® (TUNEL)	Millipore	S7101		N.A.
4-hydroxynonenal (4-HNE)	Abcam	ab-48506	Ms MC	1:1000
Kidney injury molecule-1 (KIM-1)	R & D Systems	AF1817	Gt PC	1:400
Lotus tetragonolobus agglutinin	Vector	B1325		N.A.
Megalin/Lrp2	Abcam	ab-76969	Rb PC	1:200
Nestin	Millipore	MAB353	Ms MC	1:200
NBT (nitroblue tetrazolium)	Sigma-Aldrich	N5514		N.A.
Picrosirius Red	Polysciences	09400		N.A.
Renin	Gift from Dr.Tadashi Inagami/Vanderbilt U.		Gt PC	1:12,000
α-Smooth-Muscle Actin	Sigma-Aldrich	A-2547	Ms MC	1:800
Transgelin	Gift from Dr. ShuMan Fu /U. Virginia		Rb PC	1:1500
Vimentin	Abcam	ab-45939	Rb PC	1:2500

586

587 (Abcam/Cambridge, MA; Cell Signaling Technology/Beverly, MA; Enzo Life
588 Sciences/Farmingdale, NY; Millipore/Temecula,CA; Polysciences/Warrington, PA; R & D
589 Systems /Minneapolis MN; Santa Cruz Biotechnology/Santa Cruz, CA; Sigma-Aldrich/St.
590 Louis, MO; Vector Laboratories/Burlingame, CA)

591

Figure Legends

Figure 1. Comparison of the glomerulotubular junction and initial segment of the proximal tubule in 6-10 month-old wild-type C57BL/6 (*left-hand column*) and Ctns $^{-/-}$ mice (*right-hand column*).

A, B: "Semithin" plastic sections of glutaraldehyde-perfused kidneys. In **A**, the typical configuration, in which columnar or cuboidal epithelial cells, similar in their mitochondrial content to the contiguous proximal-tubule cells, form part of Bowman's capsule, making an abrupt transition (*arrows*) to flattened parietal cells. **B** shows a glomerulus with the cystinotic "swan-neck lesion," (SNL) in which Bowman's capsule and the initial proximal-tubule segment alike consist of flat, mitochondrion-poor epithelial cells, which—beginning in the glomerulotubular junction—have generated a thickened basement membrane (*). Scale bar in **B** = 25 μm and applies to both **A** and **B**.

C, D: Kidneys perfused with nitroblue tetrazolium (NBT), which generates a precipitate of blue diformazan crystals resulting from superoxide produced by mitochondrial metabolic activity. In **C**, diformazan is deposited on the basal surfaces of tall, mitochondrion-rich epithelial cells of the glomerulotubular junction and proximal tubule (note the grazing section of a proximal tubule at lower right). By comparison, the cystinotic nephron in **D** lacks any diformazan crystals, though an adjacent downstream proximal tubule segment that retains its normal morphology shows incorporated crystals.

E, F: *Lotus tetragonolobus* staining marks the apical cytoplasm of the tall epithelial cells of glomerulotubular junction and proximal tubule in **E**, corresponding to the location of the endocytic ("tubulovesicular") system in those cells. In **F**, lectin positivity is retained only where tall cells persist, and is absent from the flattened cells of the SNL.

G, H: Immunostaining for the receptor molecule megalin, which closely resembles the *Lotus* pattern seen in wild-type mice (**G**, cf. **E**), but is retained in both flattened and tall cells of the SNL (**H**). Scale bar in **H** = 50 μm and applies to panels **C**-**H**.

I, J: Basement membrane thickness compared, as demonstrated by PAS staining. Whereas the wild-type nephron (**I**) bears a uniformly thin coating, the cystinotic (**J**) is invested with a noticeably thicker one (*arrowheads*) along the flattened epithelial-cell segment. Scale bar in **J** = 50 μm and applies to both **I** and **J**.

Figure 2. Initiation and progression of the swan-neck lesion (SNL) in the *Ctns*$^{-/-}$ mouse. Panels **A**-**D** show differing stages of alteration as emphasized by *Lotus* lectin staining, beginning as tall, lectin-positive epithelium (**A**) followed by cell flattening and a loss of lectin affinity that begins at the glomerulotubular junction (**B**) and extends distally (**C**, **D**) to form the definitive "swan-neck lesion." However, all four micrographs are from a 6-month-old animal, demonstrating the heterogeneity of nephron morphology that is typical at this age and beyond. Scale bar in **D** = 50 μm and applies to panels **A**-**D**.

The graph in E demonstrates the maturation of the glomerulotubular junction in wild-type mice (*blue symbols*) and cystinotic mice (*red symbols*), showing that both strains have a similar rate of maturation in the first month of life, while *Ctns*$^{-/-}$ mice fail by three months to achieve the same incidence of tall, *Lotus*-positive epithelial cells within glomerular capsules. Whereas wild-type mice maintain nearly 90% *Lotus*-positive glomerular cells throughout life, the fraction of *Lotus*-positive glomeruli in *Ctns*$^{-/-}$ mice decreases progressively after 3 months, leaving less than 20% at 9 months of age ($p<0.001$ vs. wild-type). This represents the rate of *initiation* of the SNL at the glomerulotubular junction. The process is shown schematically in **F-J**: In the first month of life (**F**), the majority of glomeruli are immature and lack *Lotus* staining, regardless of strain. With progressive

maturation, the fraction of *Lotus*-positive mature glomeruli increases and remains stable in wild-type mice (**G and H**). In cystinotic mice, however, initiation of the SNL is superimposed on the maturing nephron population (**I**) and this proceeds heterogeneously with advancing age (**J**).

Figure 3. Mitoquinone (MitoQ) delays initiation of the swan-neck lesion (SNL) in the *Ctns*$^{-/-}$ mouse. To test the contribution of oxidative injury to the initiation of the SNL, *Ctns*$^{-/-}$ mice were treated with vehicle (decyl-triphenylphosphonium, dTPP) or Mitoquinone (MitoQ, an antioxidant targeted to mitochondria) added to drinking water. Mice were treated from 3 to 6 months of age (short-term, dTPP, n=8, or MitoQ, n=9), and from 1 to 6 months of age (long-term, dTPP, n=9, or MitoQ, n=9) (**A**). Kidneys from all mice were harvested at 6 months of age, and fraction of intact glomerulotubular junctions (*Lotus* lectin-positive glomeruli) and proximal tubular volume fraction (*Lotus*-positive cortical tubules) were determined (**B** and **C**). Because results of short- and long-term treatment did not differ, data for the fraction of both were combined for each treatment group. Short-term treatment, green circles; long-term treatment, brown triangles; dTPP, open symbols; MitoQ, filled symbols.

Figure 4. Glomerulotubular functional anatomy is retained in cystinotic nephrons.

A, B. Juxtaglomerular apparatus. The semithin plastic section (**A**) was stained with alcoholic basic fuchsin, its affinity for glycoproteins highlighting granules (*arrows*) in the afferent arteriolar smooth muscle that correspond to the immunohistochemical location of renin (shown in **B**).

C. Semithin plastic section of a glomerulus and associated swan-neck lesion. The glomerular tuft appears normal, as does the macula densa (*MD*) at left . Scale bar in **B** applies to both **A** and **B** and = 50 μm; scale bar in **C** = 50 μm.

Figure 5. Glomerulotubular remodeling in 9 month-old mouse kidneys: Transgelin and α-smooth muscle actin (α-SMA). Transgelin staining in a wild-type kidney is localized primarily to vascular smooth muscle (*VSM*), with only limited staining of glomerular capsules (*arrowhead*) (**A**). In comparison, a similarly-aged *Ctns*$^{-/-}$ kidney shows extensive transgelin positivity in glomerular capsules (**B**). In **C**, a 10 μm-thick paraffin section of a cystinotic kidney, the arteriole (at left), glomerular capsule and contiguous proximal tubule (at right) all stain intensely for transgelin. **D**, **E**. Serial 3 μm sections of a cystinotic kidney, with transgelin staining in **D**, α-SMA in **E**. Though arterioles stain with both antibodies, stronger staining is seen for transgelin than for α-SMA in a zone of crowded glomeruli and interstitial myofibroblasts. **F**, **G**. Details of the serial sections, with the same glomerulus demonstrating both transgelin (**F**) and α-SMA (**G**) staining in its capsule epithelium. Scale bar in **B** = 100 μm and applies to **A** and **B**; scale bar in **C** = 50 μm; scale bar in **E** = 100 μm and applies to **D** and **E**; scale bar in **G** applies to both **F** and **G** and = 50 μm.

Figure 6. The fate of proximal tubules in cystinotic kidneys. Representative views of *Lotus*-stained outer cortex are shown in **A-D**, illustrating the rarefaction of labeled proximal tubules with aging, attributable both to SNL formation and loss of nephrons at later stages. The *Lotus* lectin-staining volume fraction of proximal tubules increases rapidly with maturation in both wild-type and *Ctns*$^{-/-}$ mice in the first 3 months of life (**E**). After 6 months of age, however, the volume fraction of *Lotus*-stained proximal tubules falls below that of age-matched wild-type mice ($p<0.001$) (**E**). Scale bar in **D** = 250 μm. Blue triangles, wild-type; red triangles, *Ctns*$^{-/-}$ mice.

Figure 7. Late response to injury: degeneration of proximal tubules in *Ctns*$^{-/-}$ kidneys (A-D, 9 month-old kidneys). Degenerative changes in delimited areas containing shrunken tubules include apoptosis revealed by TUNEL-staining (**A**), evidence of superoxide generation (blue diformazan crystals within epithelial cells) (**B**), kidney injury molecule-1 (KIM-1) (**C**) and 4-hydroxynonenal (4-HNE) (**D**). Note apoptotic figures (*arrows*) in **C** and **D**. **E** and **F**: Papillary intratubular cast material accumulates with age in the cystinotic mouse kidney. Cast material is sparse at 3 months (**E**) whereas by 20 months (**F**) many of the collecting ducts are filled with PAS-positive casts Scale bar in **D** = 50 µm and applies to all panels. Scale bar in **F** = 100 µm and applies to **E** and **F**.

Figure 8. Late response to injury: formation of atubular glomeruli. Panel **A** is a survey of an extensive degenerative zone in a 14-month-old cystinotic mouse kidney. Masses of monocellular infiltrate (*), tubules filled with cast material (*CM*), and groups of crowded glomeruli, many with dilated Bowman's spaces, are characteristic of such lesions. The expansion of Bowman's space is demonstrated in **B**, comparing typical glomeruli in *Ctns*$^{-/-}$ mice at 3 months versus 20 months of age. There is a progressive increase in Bowman's space after 12 months of age (**B**). Serial consecutive sections (arranged vertically) through a glomerulus from a 20 month-old *Ctns*$^{-/-}$ mouse demonstrates the termination of the initial segment of the proximal tubule in a blind end (*arrows* in panels 6-8), thus constituting an "atubular glomerulus" (**C**). Scale bar in **A** = 250 µm; scale bar in **B** = 100 µm and applies to both panels. Scale bar in **C** = 100 µm and applies to all panels.

Figure 9. Late response to injury: interstitial collagen deposition. A. PAS staining shows intense positivity within the thickened coatings of shrunken tubules (examples at *arrows*) in a 14-month-old *Ctns*$^{-/-}$ mouse kidney. Expressed as a fraction of total parenchymal area,

718 picrosirius red staining remains less than 3% for the first 6 months of life, followed by a
719 sharp increase thereafter (**B**). **C**. Picrosirius red-staining collagen follows a similar
720 distribution localized to basement membrane of Bowman's capsule at 3 months, and
721 extending to tubular basement membranes by 20 months. This suggests that the
722 measured collagen is primarily type IV, rather than representing the more typical fibrosis
723 comprised of interstitial type I collagen fibril depositions. Scale bar in **A** = 100 μm; Scale
724 bar in **C** = 250 μm and applies to both panels.
725
726 **Figure 10. Progression of cystinosis in mouse and man.** A natural history of human
727 cystinosis can be constructed from the few available reports describing renal function and
728 morphology from infancy to adulthood. Fanconi syndrome generally develops in the first 6
729 months of life, with significant decrease in GFR by 2 to 5 years, and renal failure in the
730 second decade. There is marked inter-individual variability in the rate of progression of
731 renal lesions, and treatment with cysteamine can significantly delay progression to renal
732 failure. The evolution of renal lesions in the mouse is more gradual, with GFR decreasing
733 only later in adulthood. The period of proximal tubular maturation extends through the first
734 6 months in man and the first 3 months in the *Ctns*$^{-/-}$ mouse; the "swan-neck lesion" is
735 initiated in the first 3 months in the mouse, and between 6 and 12 months in man. The
736 development of irreversible renal lesions in both species includes loss of functional
737 proximal tubular mass and the development of tubular atrophy, interstitial fibrosis and
738 formation of atubular glomeruli. Therapy should be directed to the early period of
739 adaptation (potentially reversible changes) rather than the late (destructive) phase.
740

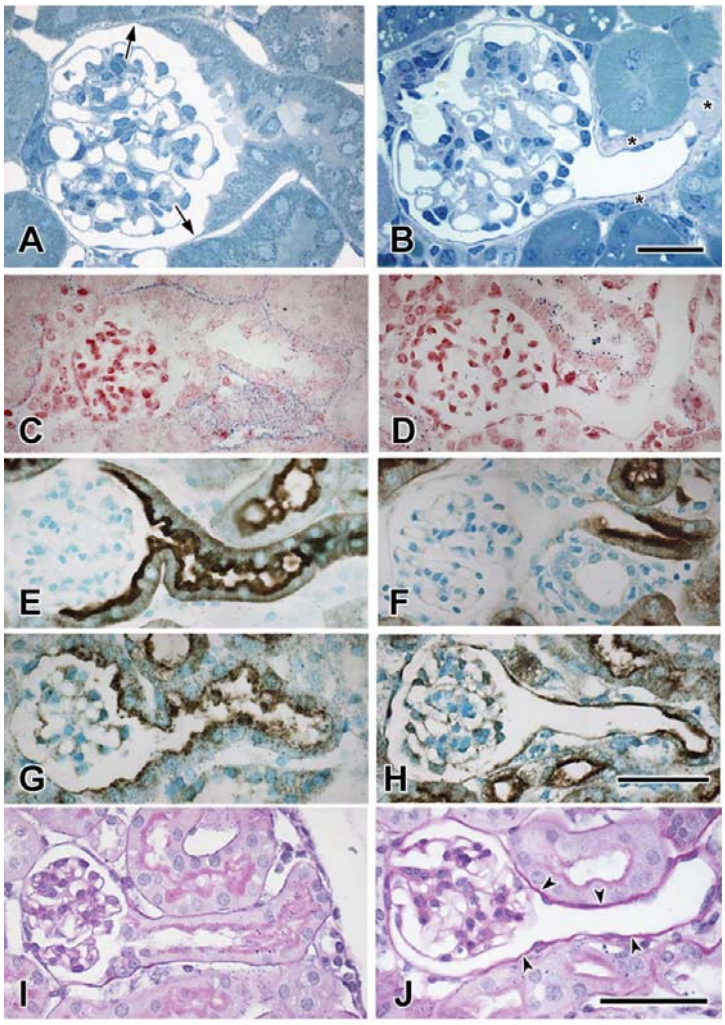

Figure 1

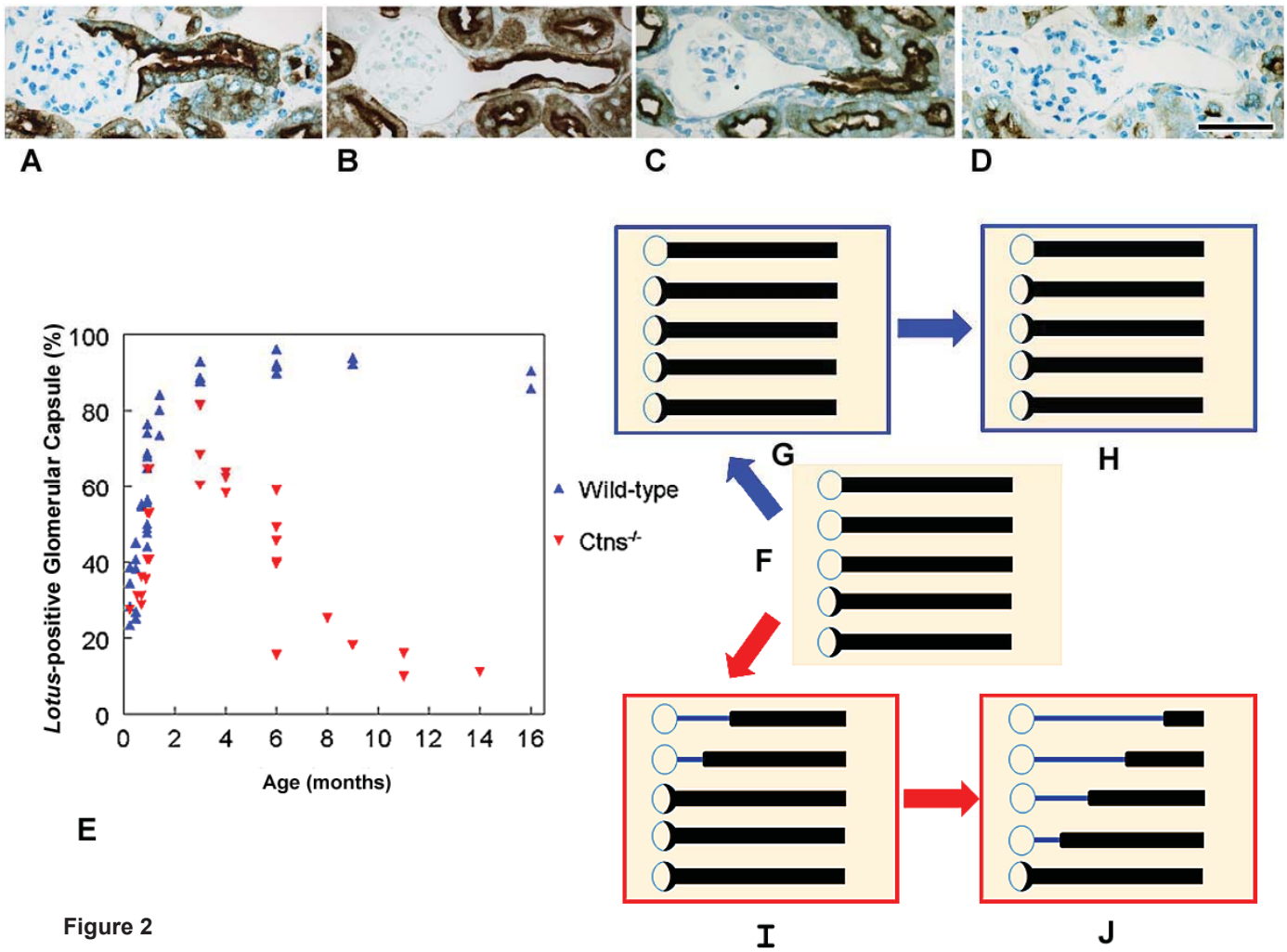
A
B
C
D
Lotus-positive Glomerular Capsule (%)
100
80
60
40
20
0
0
2
4
6
8
10
12
14
16
Age (months)
Wild-type
Ctns-/-
E
G
H
F
I
J

Figure 2

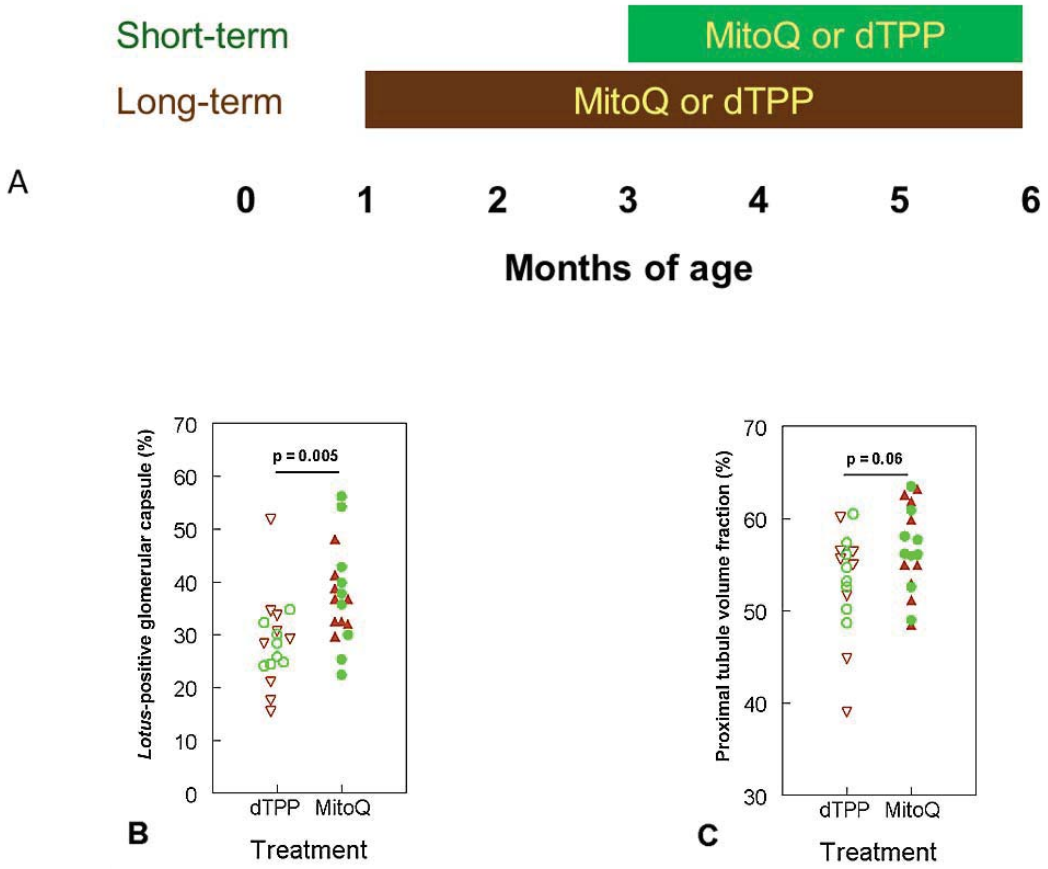
Short-term
MitoQ or dTPP
Long-term
MitoQ or dTPP
A
0
1
2
3
4
5
6
Months of age
Lotus-positive glomerular capsule (%)
p = 0.005
dTPP
MitoQ
Treatment
B
Proximal tubule volume fraction (%)
p = 0.06
dTPP
MitoQ
Treatment
C

Figure 3

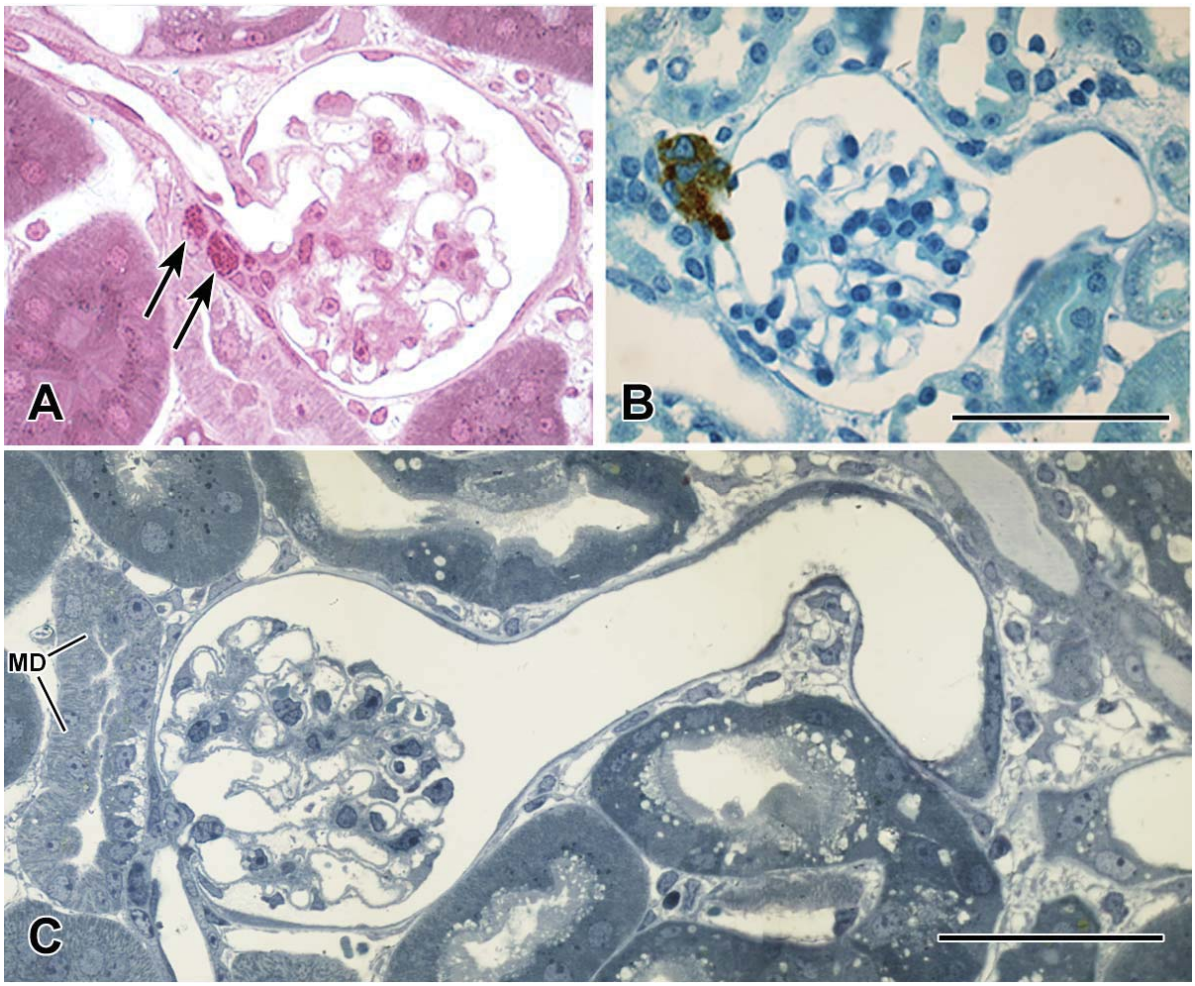

Figure 4

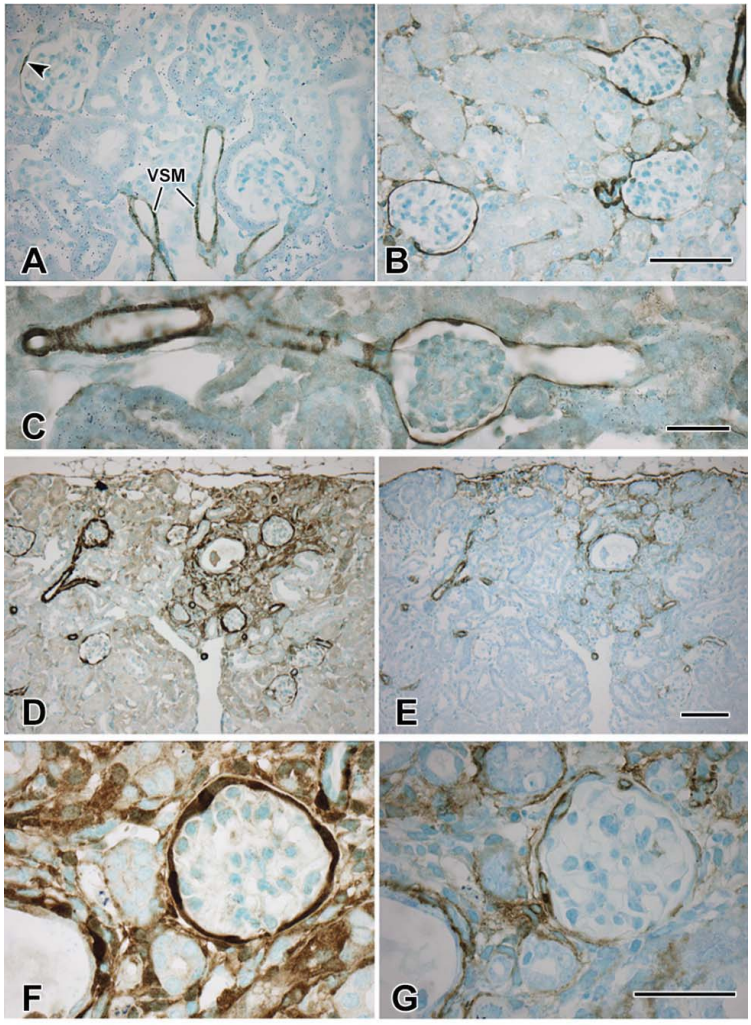

Figure 5

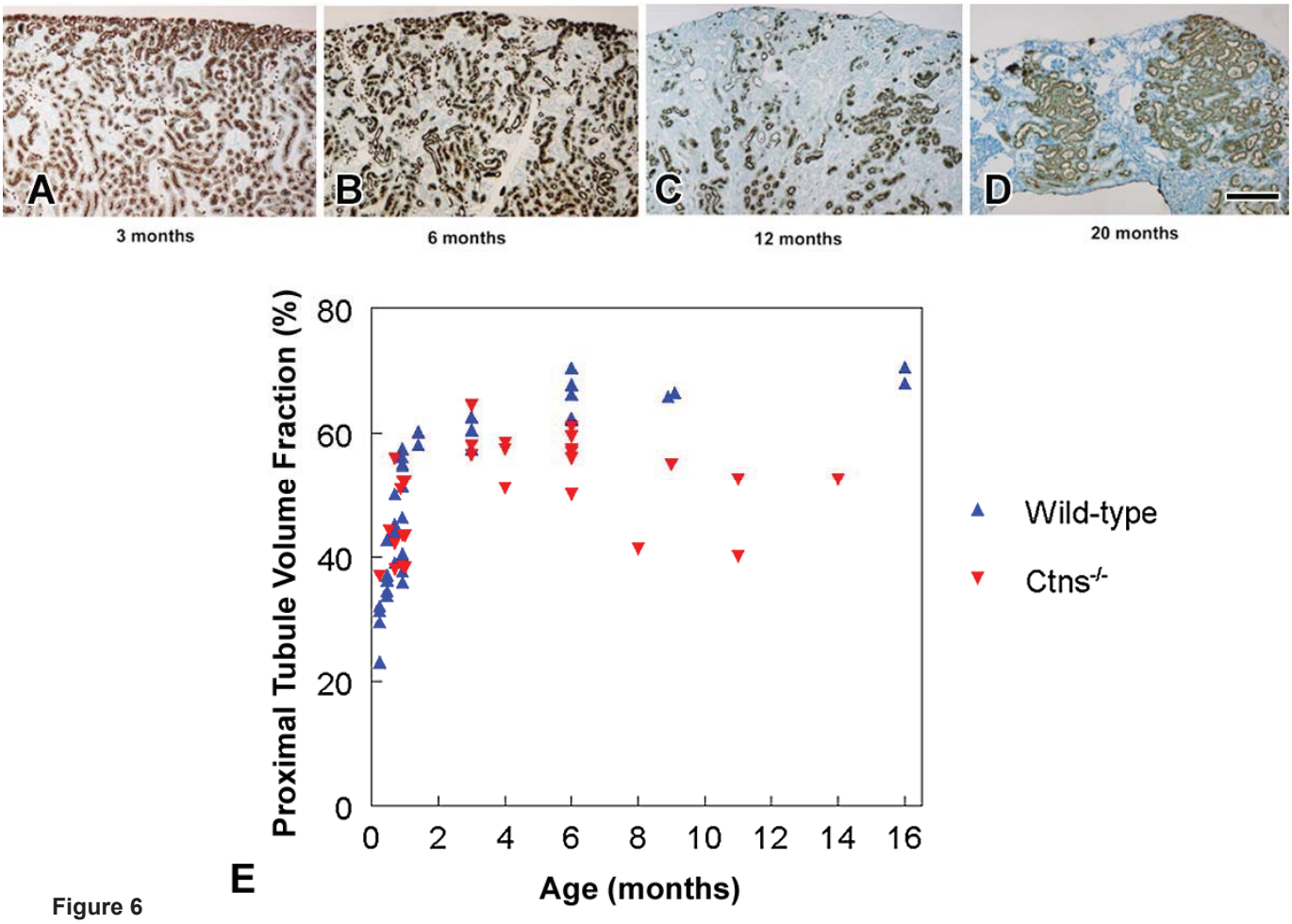
A
B
C
D
3 months
6 months
12 months
20 months
Proximal Tubule Volume Fraction (%)
80
60
40
20
0
0
2
4
6
8
10
12
14
16
Age (months)
Wild-type
Ctns-/-
E

Figure 6

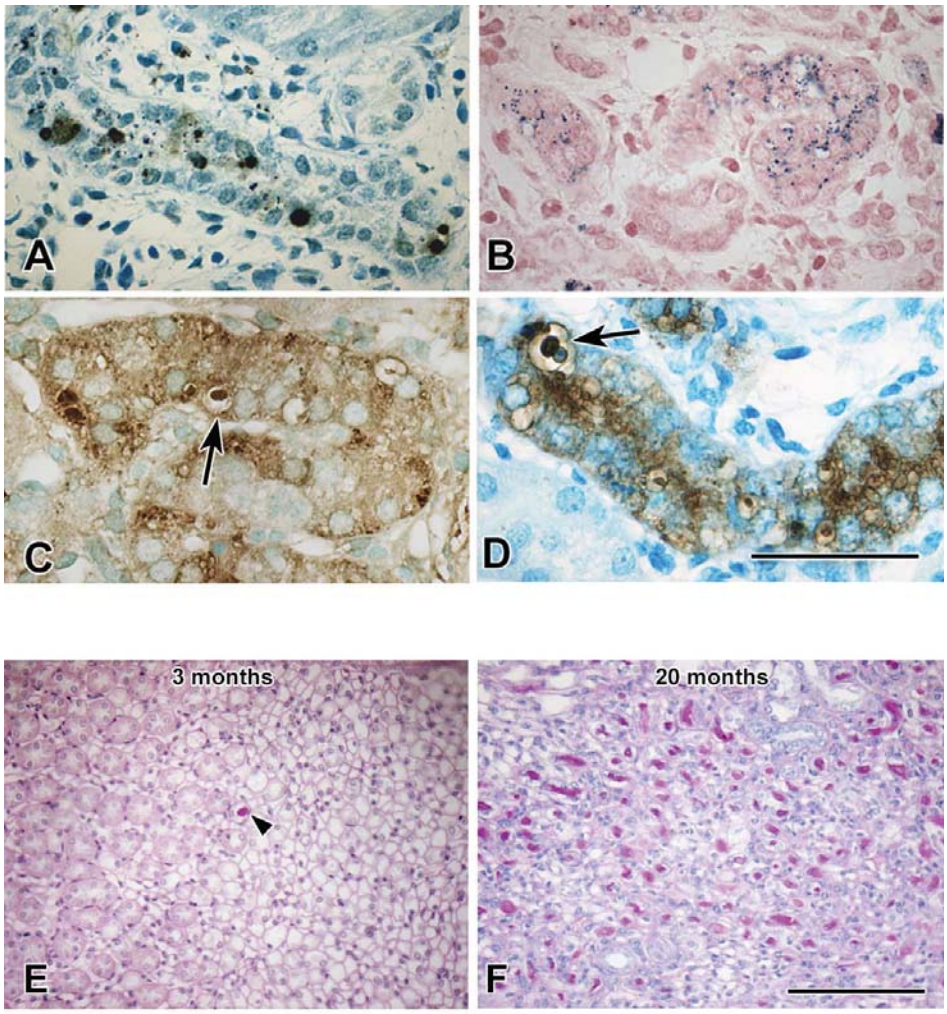

Figure 7

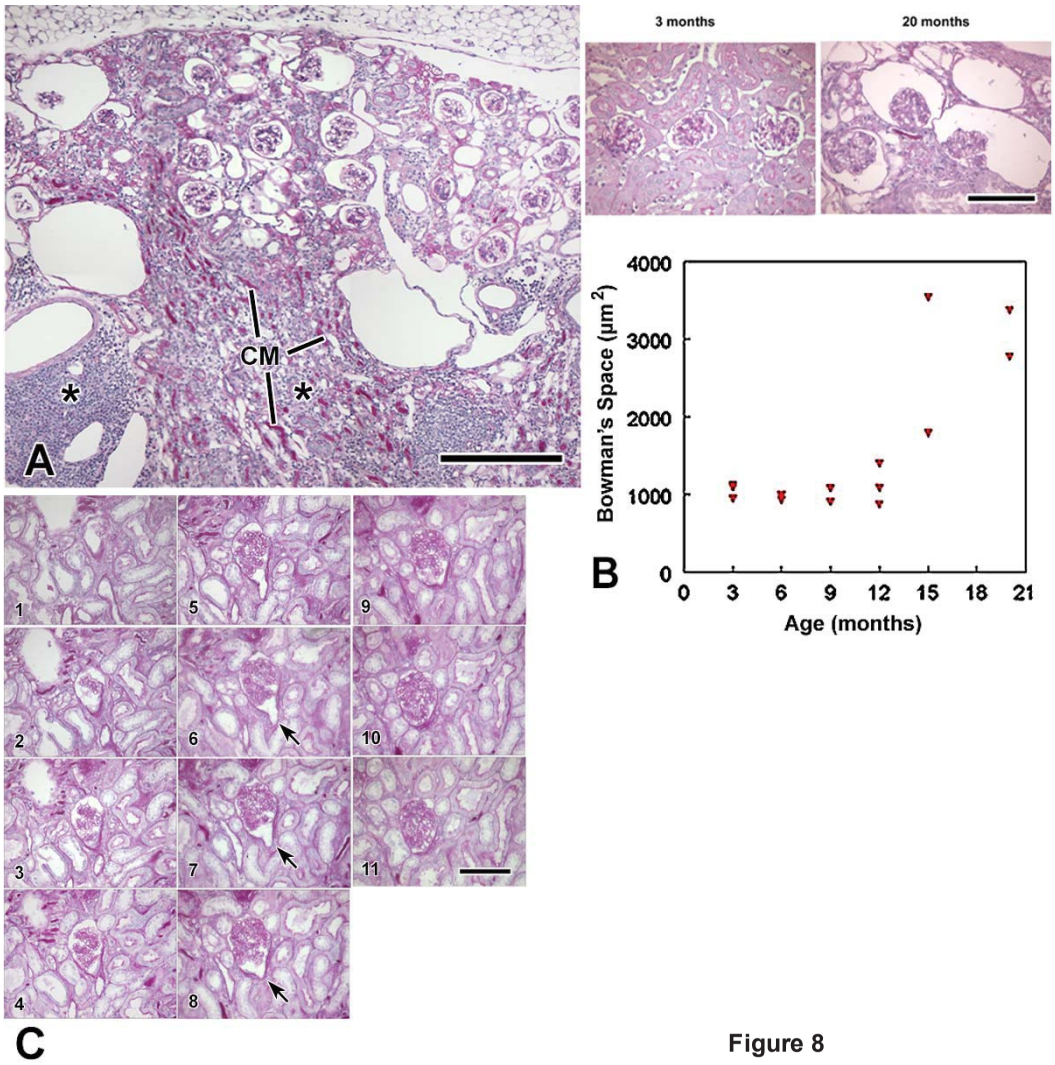
A
CM
*
*
3 months
20 months
B
Bowman's Space (µm 2)
4000
3000
2000
1000
0
0
3
6
9
12
15
18
21
Age (months)
1
2
3
4
5
6
7
8
9
10
11
C

Figure 8

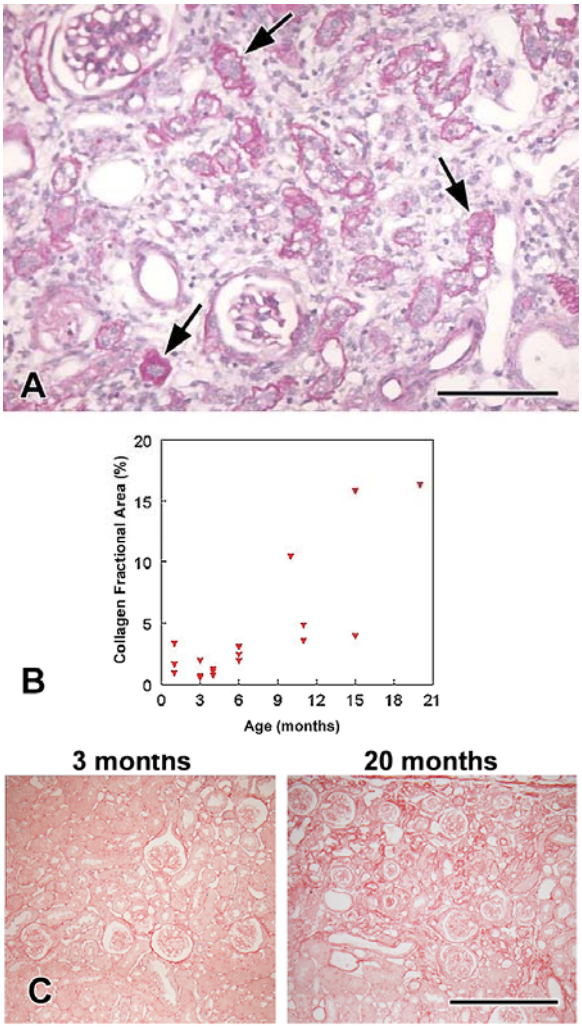
A
B
Collagen Fractional Area (%)
0
5
10
15
20
0
3
6
9
12
15
18
21
Age (months)
3 months
20 months
C

Figure 9

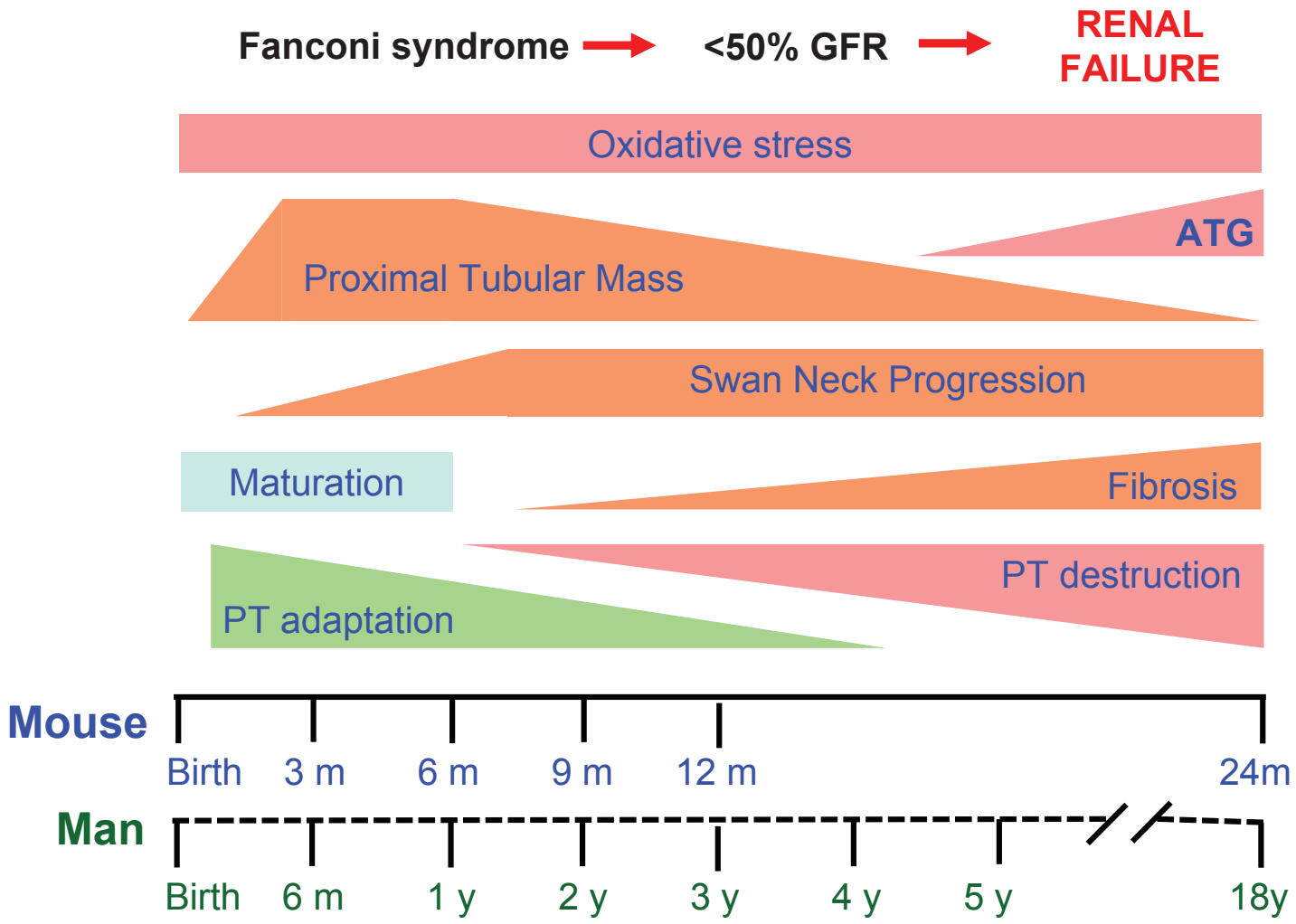
Fanconi syndrome
<50% GFR
RENAL FAILURE
Oxidative stress
ATG
Proximal Tubular Mass
Swan Neck Progression
Maturation
Fibrosis
PT destruction
PT adaptation
Mouse
Birth
3 m
6 m
9 m
12 m
24m
Man
Birth
6 m
1 y
2 y
3 y
4 y
5 y
18y

Figure 10